Supplementary Information (SI) Appendix for "Two-axis control of a singlet-triplet qubit with an integrated micromagnet"

Xian Wu,[1] D. R. Ward,[1] J. R. Prance,[2] Dohun Kim,[1] John King Gamble,[1] R. T. Mohr,[1] Zhan Shi,[1] D. E. Savage,[1] M. G. Lagally,[1] Mark Friesen,[1] S. N. Coppersmith,[1] and M. A. Eriksson[1]

[1] *University of Wisconsin-Madison, Madison, WI 53706*
[2] *Lancaster University, Lancaster, United Kingdom*

This supplement presents methods used to calibrate the detuning energy (lever-arm α) and to convert measurements of time-averaged current through the quantum point contact (QPC) to probabilities of being in the singlet state just after a given pulse sequence has been applied, including data used to extract the spin relaxation time T_1 used in the normalization process. Data for the "ΔB" gate and the exchange gate for $\Delta B = 32$ neV are shown here. We present the results of a simulation of the X or "ΔB" gate performed with two different forms for the functional dependence of J on detuning. We also describe the fabrication of the sample and include an image of the micomagnet.

CALIBRATION OF DETUNING ENERGY

We find the conversion between the detuning voltage V_ε and the detuning energy ε from measurements of the charge stability diagram under non-zero source-drain bias, as shown in Fig S1(a). We apply -200 μV between the right dot reservoir and the left reservoir, to raise the Fermi level of the right reservoir 200 μeV higher than that of the left reservoir. By drawing the charge transition lines on top of the stability diagram, as shown in Fig. S1(b), we can measure the shift in gate voltage of charge transitions arising from the 200 μeV potential difference between the two reservoirs. Because of the applied bias, the two triple points turn into triangles. The highlighted points are useful for converting dot energies to gate voltages. Each point has its energy level diagram drawn, as shown in Figs. S1(c-f). Moving from the yellow point to blue point in gate voltage will raise both dot potentials by 200 μeV. Adjusting gate voltages from the yellow point (or blue point) to the green point will create a 200 μeV energy difference between the dots. The detuning direction we used is labeled with a yellow arrow, from the red point to green point, creating 200 μeV energy difference by moving each dot potential in opposite directions by the same amount. The voltage changes measured are 4 mV on LP and -4 mV on RP, corresponding to $4\sqrt{2}$ mV in the detuning direction. Thus the conversion factor is $4\sqrt{2}$ mV in detuning voltage for each 200 μeV in detuning energy, corresponding to $\alpha = 35.4$ μeV/mV.

METHOD OF CONVERSION OF THE QPC CURRENT MEASUREMENT TO PROBABILITY OF BEING IN THE SINGLET STATE

Here we present the methods used to convert measurements of the time-averaged difference in QPC current ($\Delta I_{\rm QPC}$) to probabilities of being in the singlet state just after a given pulse sequence has been applied. The method is similar to the one described in the supplemental material of Ref. [1], except for the pulse sequence used in the extraction of the $\Delta I_{\rm QPC}$ that corresponds to the one electron change (0,2) to (1,1).

All the pulse sequences are generated by a Tektronix AFG3250 pulse generator. The reference lockin signal is a square wave with frequency of either 67 or 111 Hz (red dashed trace in Fig. S2(a)). During one half of a cycle, a pulse train is applied to the gates of the quantum dots (purple trace in Fig. S2(a)). The lockin signal $\Delta I_{\rm QPC}$ measures the change in the average charge occupation induced by the application of the pulses. The averaging time for each data point is two seconds. To convert the measured $\Delta I_{\rm QPC}$ to singlet probability $P_{\rm S}$, we note that the charge state at the end of the pulse is (1,1) for a spin triplet, while it is (0,2) for a spin singlet. If the spin state is a triplet at the end of a pulse, it will relax back to the singlet in a time T_1. Therefore,

$$P_{\rm S} = 1 - \frac{\Delta I_{\rm QPC}}{\Delta I_1} \cdot \frac{T_1}{T_{\rm m}} \cdot \left(1 - \exp\left(-\frac{T_{\rm m}}{T_1}\right)\right), \qquad \text{(S1)}$$

where ΔI_1 is the value of $\Delta I_{\rm QPC}$ that corresponds to a one electron change from ((0,2) to (1,1)), and T_1 is the relaxation time of $T(1,1)$ to $S(0,2)$. We measure ΔI_1 by sweeping gate voltage along the detuning direction while applying the pulses shown in Fig. S2(a). Fig. S2(b) shows the lockin response as a function of detuning; the maximum change in $\Delta I_{\rm QPC}$ is ΔI_1.

The spin relaxation time T_1 for the T_- state is extracted by measuring the S-T_- oscillation amplitude as a function of $T_{\rm m}$, the time between successive pulses in the pulse train. Three traces of S-T_- oscillations are shown in Fig. S2(c); they demonstrate that the oscillation amplitude decays with increasing $T_{\rm m}$, as expected. The oscillation amplitude as a function of $T_{\rm m}$ satisfies

$$\Delta I_{\rm QPC} = A \cdot \frac{T_1}{T_{\rm m}} \cdot \left(1 - \exp\left(-\frac{T_{\rm m}}{T_1}\right)\right), \qquad \text{(S2)}$$

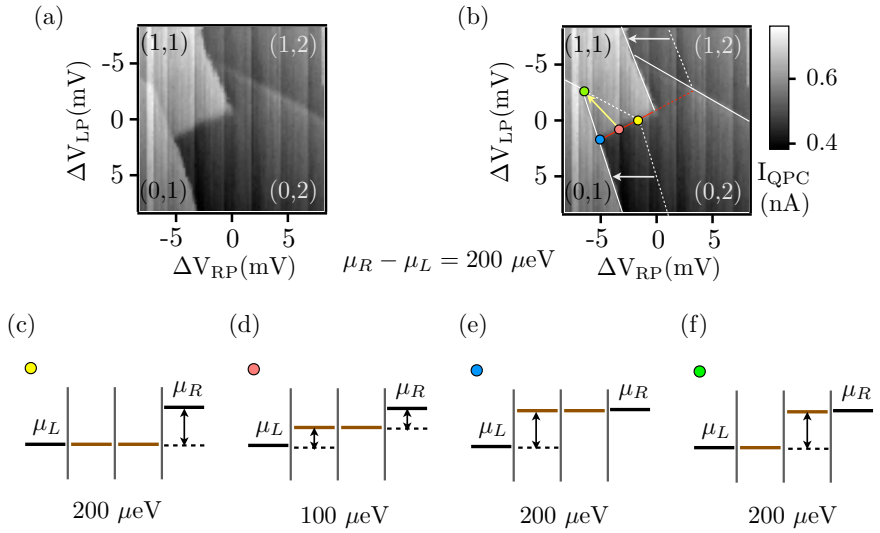

FIG. S1. (a) Charge stability diagram with -200 μV right dot reservoir bias voltage applied. Electron occupation numbers are labeled. (b) Same charge stability diagram as (a), with charge transition lines superimposed. A 200 μeV potential difference between left and right dot reservoirs shifts the right dot transitions ~ -4 mV on gate RP (see arrows). (c)-(f) Energy level diagrams showing energies for each dot and reservoir correspond to the four positions highlighted in (b). Energy differences are labeled and listed for each case.

where A is a time-independent coefficient. Fig. S2(d) shows the oscillation amplitude as a function of $T_{\rm m}$; a fit to Eq. (S2) yields $T_1 = 9.85 \pm 1.19$ μs.

To measure the spin relaxation time T_1 for the T_0 state, we measure as a function of $T_{\rm m}$ the value of $\Delta I_{\rm QPC}$ when we pulse into (1,1) for a time $\tau_{\rm s}$ significantly longer than the singlet-triplet T_2^*, so that S and T_0 are completely mixed ($\tau_{\rm s} > 2T_2^*$). The relaxation time for the T_0 state again obeys Eq. (S2). Fig. S1(e) and (f) show measurements of $\Delta I_{\rm QPC}$ a a function of $T_{\rm m}$ along with the fit to Eq. (S2) used to extract this T_1.

DATA FOR SMALLER ΔB THAN IN MAIN TEXT

Fig. S3 reports data showing oscillations in the singlet probability corresponding to the "ΔB" gate and the exchange gate for $\Delta B = 32$ neV. The pulse sequences used here are the same as those shown in Fig. 2(b) and Fig. 3(a) in the main text.

SIMULATION OF THE X OR "ΔB" GATE

Fig. S4 reports the results simulations of the "ΔB" gate with two different functional forms for the dependence of J on detuning, with the details described in the caption. We find that J appears to vary exponentially as a function of detuning energy, in agreement with previous observations by Dial et al. [2].

MICROMAGNET FABRICATION

An optical micrograph of the device including the micromagnet is shown in Fig. S5. The micromagnet is 12.64 μm × 1.78 μm × 242 nm. The magnet was patterned via electron-beam lithography on top of the accumulation gates approximately 1.78 μm to the left and 122 nm above the center of the two quantum dots. The magnet was deposited via electron-beam evaporation with a metal film stack of 2 nm Ti / 20 nm Au / 200 nm Co / 20 nm Au evaporated at approximately 0.3 Å/s. The gold film is intended to help minimize oxidation of the Co film.

[1] D. Kim, Z. Shi, C. B. Simmons, D. R. Ward, J. R. Prance, T. S. Koh, J. K. Gamble, D. E. Savage, M. G. Lagally, M. Friesen, S. N. Coppersmith, and M. A. Eriksson, "Quantum control and process tomography of a semiconductor quantum dot hybrid qubit," (2014), preprint arXiv:1401.4416.

[2] O. E. Dial, M. D. Shulman, S. P. Harvey, H. Bluhm, V. Umansky, and A. Yacoby, Phys. Rev. Lett. **110**, 146804 (2013).

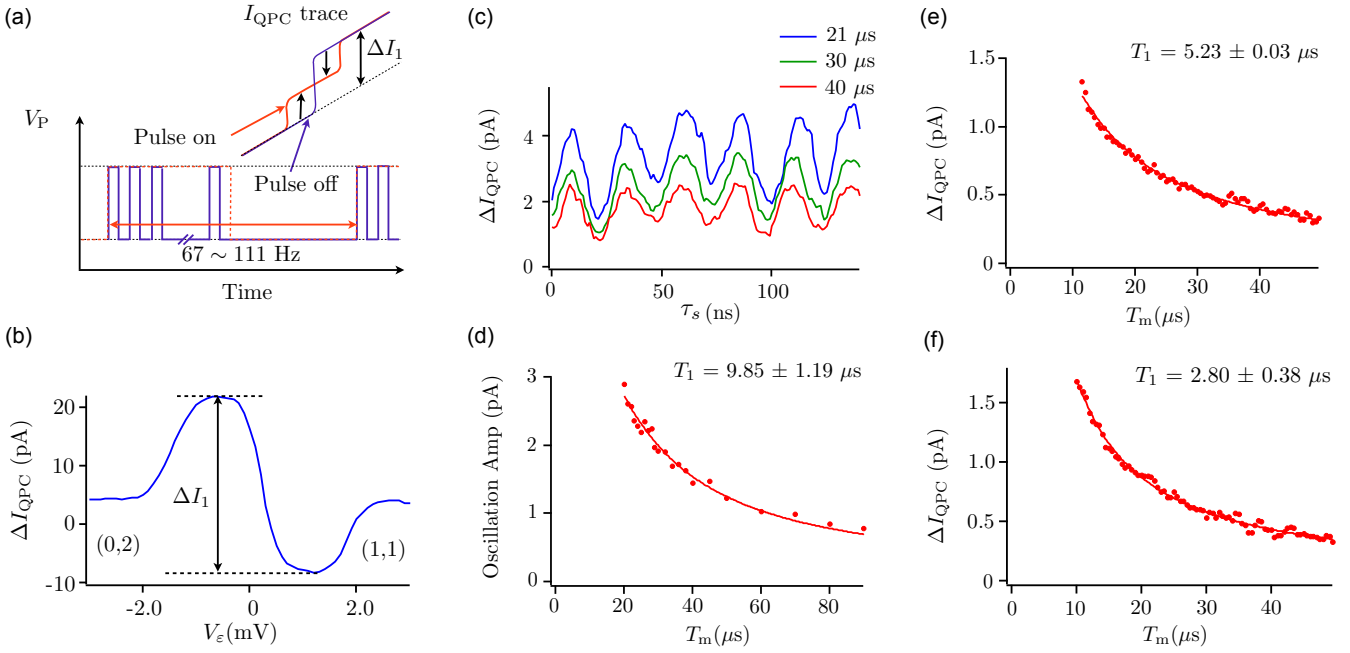

FIG. S2. Measurements used to determine the relationship between the lockin signal ΔI_{QPC} and the probability of being in the singlet state after application of a given pulse sequence, using Eq. (S1). (a) Pulse sequence used to measure ΔI_{QPC} that corresponds to one electron change from (0,2) to (1,1). The red dashed line indicates the low frequency signal used as the lockin reference. The square pulses shown in purple inside the red dashed line have the same frequency as the actual manipulation pulse used in the experiment. Inset: schematic diagram showing the expected dc value of I_{QPC} during the 1/2 cycle with pulses applied (red) and the 1/2 cycle with pulses not applied (purple). The black arrow indicates the maximum measured lockin signal ΔI_1 (see panel (b)). (b) ΔI_{QPC} measured as we sweep gate voltage along detuning with the above pulse sequence applied. (c) Three traces of ΔI_{QPC} as a function of pulse width τ_s are shown, exhibiting S-T_- oscillations. The three traces are acquired with three different values of the time T_{m} between successive pulses. The oscillation amplitude decreases significantly with T_{m}, indicating that relaxation to (0,2) occurs on a time scale shorter than 20 μs. (d) S-T_- oscillation amplitude plotted as a function of T_{m}. The corresponding value of T_1 is used to normalize the data shown in Fig. 1(h) in the main text. The solid line is a fit to Eq. (S2), which yields the relaxation time T_1 shown on the figure. (e),(f) Measurement of the spin relaxation time T_1 for the T_0 state. For this measurement, a pulse is applied into (1,1) that is significantly longer than the inhomogeneous dephasing time T_2^*, so that the state at the end of the pulse is an equal mixture of S-T_0. The decay of ΔI_{QPC} with T_{m}, the time between successive pulses, obeys Eq. (S2). The value of T_1 extracted by fitting to Eq. (S2) is listed on the plot. T_1 from (e),(f) are used to convert ΔI_{QPC} to singlet probability for Fig. 2(c) and Fig. 3(c), respectively, in the main text.

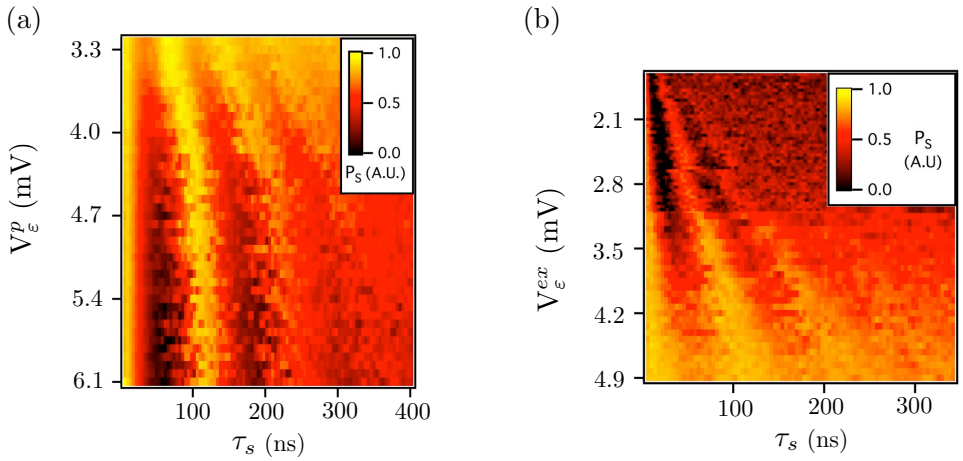

FIG. S3. Data corresponding to the "ΔB" gate and the exchange gate for $\Delta B = 32$ neV. (a) Singlet probability P_S, measured as a function of pulse duration and voltage level at pulse tip, V_ε^p. (b) Singlet probability P_S, measured as a function of pulse duration and pulse level V_ε^{ex} in the exchange pulse sequence. The singlet probability is reported in arbitrary units in both (a) and (b).

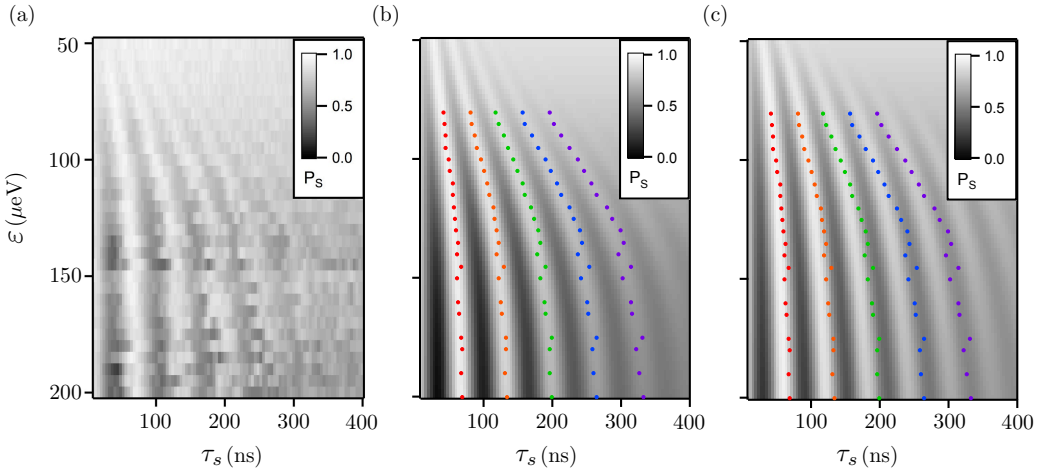

FIG. S4. "ΔB" gate data compared to simulation results using different functional forms for the dependence of J on detuning. (a) Experimentally measured singlet probability P_S plotted as a function of pulse duration τ_s and detuning energy ε at the pulse tip (Fig. 2(c) from the main text). Line cuts of data are fit to products of sinusoids and Gaussians, and the resulting maxima from the fits are plotted as colored dots in panels (b) and (c). (b) Simulation of singlet probability P_S as function of duration τ_s and detuning energy ε using $J = J_0 \exp(-\varepsilon/\varepsilon_0)$, where the best fit is found with $\varepsilon_0 = 62.7$ μeV. (c) Simulation of singlet probability P_S as function of duration τ_s and detuning energy ε using $J = \sqrt{\varepsilon^2/4 + t_c^2} - \varepsilon/2$, where the best fit is found with $t_c = 2.48$ μeV. Oscillation peaks extracted from (a) are plotted on top of (b) and (c), and the comparison suggests that $J = J_0 \exp(-\varepsilon/\varepsilon_0)$ fits the data well.

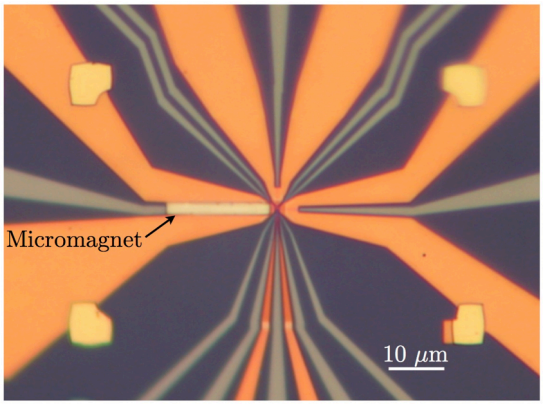

FIG. S5. Optical micrograph of the device, with the location of the micromagnet marked on the figure.